Journal of Heat and Mass Transfer Research

Journal homepage: https://jhmtr.semnan.ac.ir

Semnan University

ISSN:2383-3068

Research Article

A Semi Analytical Study on Non-Linear Boundary Value Problem for MHD Fluid Flow with Chemical Effect

Gandhirajan Petchiammal [a], Vembu Ananthaswamy [b*]

[a] *Department of Mathematics, V. H. N. Senthikumara Nadar College (Affiliated to Madurai Kamaraj University), Virudhunagar, Tamil Nadu, India*

[b] *Research Centre and PG Department of Mathematics, The Madura College (Affiliated to Madurai Kamaraj University), Madurai, Tamil Nadu, India*

ARTICLE INFO

Article history:

Received: 2023-12-20

Revised: 2024-06-18

Accepted: 2024-06-18

Keywords:

Boundary value problem ;
Chemical reaction;
Heat and mass transfer;
Homotopy analysis method;
MHD fluid flow ;
Micropolar fluid.

ABSTRACT

The Runge-Kutta method combined with the shooting technique is used to solve the numerical results of the theoretical model for the electrically conducting micropolar fluid through two parallel plates in the presence of a heat source or sink and first-order chemical reactions in the flow heat and mass transfer equations. This work encourages us to use the Homotopy analysis approach to develop semi-analytical solutions for dimensionless velocity, dimensionless microrotation, dimensionless temperature, and dimensionless concentration. The answers are used to produce the analytical approximations of the physical characteristics, such as the skin friction factor, Nusselt number, and Sherwood number. Additionally, tabular values for the physical parameters, such as the skin friction factor, Nusselt number, and Sherwood number, are provided. Graphs are also used to illustrate how characterizing parameters behave. We found a high correlation between the semi-analytical and numerical findings of this study when we compared our semi-analytical works with the earlier studies. Compared to the prior method, this approach to the model is simpler, and it may be readily extended to find semi-analytical solutions to other MHD and EMHD fluid flow issues in the physical sciences and engineering.

1. Introduction

Because the topic of micropolar fluid dynamics is becoming more and more used in the processing sector, many professionals are interested in studying it. In order to account for the microstructure and the local motion of the particles inside the fluid's volume element, Erigen created micropolar fluids in 1966. Erigen [1] investigated the effects of inertial spin, local rotary inertia, and the pair stresses in order to develop a model for the non-Newtonian behavior observed in suspended fluids, such as blood, polymers, paints, lubricants, and other non-Newtonian materials.

The study of electrically conducting fluid motion in the presence of a magnetic field, or the interaction of the magnetic field and the fluid velocity of electrically conducting fluids, such as in dynamos and MHD pumps, is known as magnetohydrodynamics (MHD). A lot of studies employ MHD flow for mass and heat transfer because of the primary effect of magnetic fields. Studying analytically and numerically, nuclear reactors, MHD generators, and other engineering

*** Corresponding author.**
E-mail address:ananthu9777@gmail.com

Cite this article as:
Petchiammal, G., Ananthaswamy, V., 2024. A Semi Analytical Study on Non-Linear Boundary Value Problem for MHD Fluid Flow with Chemical Effect. *Journal of Heat and Mass Transfer Research*, 11(2), pp. 237-254.
https://doi.org/10.22075/JHMTR.2024.32722.1510

science fields now heavily rely on electrically conducting fluids.

Mishra et al. [2] examined the flow of mass MHD-free convection and heat in a micropolar fluid with a heat source. Hague et al. [3] investigated the behavior of micropolar fluids in steady MHD-free convection flow with joule heating and viscous dissipation. Rahman et al. [4] talked about the heat transmission in a micropolar fluid down an inclined permeable plate with different fluid characteristics. The unsteady MHD mixed convection flow of a micropolar fluid down inclined surfaces is studied in the study of Aurangzaib et al. [5]. In the work of Srinivasacharya, and Bindu [6], the creation of entropy in a micropolar fluid flow via an inclined channel is examined.

An impulsively begun infinite vertical porous flat plate containing a viscous, incompressible, and electrically conducting fluid in the presence of a porous material was explored in [7] to examine the impacts of MHD, Dufour, and Soret on unstable free convection and mass transfer flow. According to Soret and Dufour effects, MHD thermo solutal convection in a porous cylindrical cavity filled with Casson nanofluid was studied [8]. Mass transport and temperature variation both cause unsteady MHD convection to flow through a loosely packed porous material and into a precipitately begun perpendicular plate [9].

Researchers have been particularly interested in the study of heat and mass transfer effects in their fluid flow problems in recent years because of the significance of chemical reactions in industries during the production process. The MHD Casson nanofluid flow via a linear stretching surface in the presence of a chemical reaction coefficient and the slip condition were described by Swapna et al. [11].

By incorporating the hitherto unrecognized magnetic field effect on the flow of micropolar fluid through the two parallel plates in the presence of a heat source or sink and a first-order chemical reaction in the flow heat and mass transfer equations, respectively, the expanded work was derived by Dash et al. [12]. The firing technique was used with the fourth-order Runge-Kutta method to solve nonlinear differential equations.

The aforementioned studies forced us to investigate these kinds utilising analytical techniques because most publications have used numerical methods. For numerical study, we can refer to the numerical study of the boundary layer flow problem over a flat plate by the finite difference method [13], and the numerical study of chemical reactions and magnetic flow over a flat plate [14].

Boundary value problems in potentiometric biosensors [15], reactive gas absorption [16], several two-point non-linear elliptic boundary value problems [17], and transient current potential for redox enzymatic homogenous systems [18] can also be consulted for analytical solutions. We have already covered a number of approximate analytical solutions. An approximate solution technique that does not depend on a small parameter [19], an approximate analytical solution of a non-linear kinetic equation in a porous pellet [20], semi-analytical expressions of a non-linear boundary value problem for immobilised enzyme in porous planar, cylindrical spherical [21], non-linear mathematical models, including the Variational Iteration method [22], Homotopy Perturbation technique [23],. Homotopy perturbation method for a new non linear analytical technique [24], Homotopy perturbation method to linear and non linear Schrodinger equations [25], new homotopy perturbation method [26], Modified Adomain Decomposition technique [27], Homotopy Analysis method for non-linear problems [28], Homotopy Analysis method for Non- linear Initial Value Problem for an Autocatalysis in a continuous stirred Tank Reactor[29], Modified Homotopy Analysis method for analytical expressions of a boundary layer flow of viscous fluid[30], Semi-analytical solution of MHD free convective Jeffrey fluid flow in the presence of heat source and chemical reaction[31], Ananthaswamy Sivasankari method for solving some non-linear initial value problems in physical sciences [32], Ananthaswamy Sivasankari method for solving non-linear boundary value problem in heat transfer through porous fin [33]. Adapting techniques in the pioneering works are mentioned in Table 1. Also, several numerical techniques were utilised for resolving MHD flow issues via MATLAB regarding RK4 [36], and bvp4c [37].

In this work, the homotopy analysis method is employed to solve the equations found in [12]. The answers are used to produce the analytical approximations of the physical characteristics, such as the skin friction factor, Nusselt number, and Sheerwood number. and the results are contrasted with the numerical results. Graphs obtained through modifications of the controlling parameters are also analysed in detail.

Table 1. Comparison of Past studies with present work

Past Studies				
Reference	**Subject Matter**	**Approach**	**Study Method**	**Outcomes**
Mishra et al. [2]	Study of Heat and Mass Transfer in MHD Flow of Micropolar Fluid over a Curved Stretching Sheet	Numerical	SOR Method	External magnetic field tends to raise temperature profiles.
Ziaul Haque et al. [3]	Micropolar fluid behavior on steady MHD free convection and mass transfer through a porous medium with constant heat and mass fluxes	Numerical	Nachtsheim–Swigert iteration technique	The skin friction is larger for lighter particles and air than heavier particles and water, respectively. The micropolar fluid temperature is more for air than water.
Kasim Aurangzaib et al. [5]	The unsteady magnetohydrodynamic mixed convection flow of a micropolar fluid over an inclined plate	Numerical	Implicit finite-difference scheme	A solution could be obtained for all positive values of the buoyancy parameter λ.
Srinivasacharya et al. [6]	Entropy generation of micropolar fluid flow through an inclined channel of parallel plates with constant pressure gradient	Numerical	Spectral quasi linearization method	The entropy generation number increases with the increase in Brinkman number and angle of inclination. Further, it is observed that the increase in coupling number, Prandtl number and Reynolds number reduces the entropy generation number.
Mustapha EI Hamma et al. [9]	Numerical study of the model thermosolute natural convection in porous, isotropic and saturated media filled with Casson nanofluids (aluminum nanoparticles) under the influence of a magnetic field	Numerical	Finite volume method	An uneven decrease in the thermo solutal transfer with the increase in the Hartmann Soret and Dufour numbers.
Meenakshi et al. [10]	Dufour and Soret Effect on Unsteady MHD Free Convection and Mass Transfer Flow Past an Impulsively Started Vertical Porous Plate Considering with Heat Generation	Numerical	Implicit finite difference method	The Skin-friction coefficient Cf decreases with the decrease of Soret number Sr. The Nusselt number Nu value increases with the effect of suction parameter v_0, while it decreases with the effect of magnetic field parameter M . No change in Nu and Sh for the different values of permeability parameter λ
Dash.et al. [12]	Chemical Reaction Effect of MHD Micropolar Fluid Flow between two Parallel Plates in the Presence of Heat Source/Sink	Numerical	Runge–Kutta method along with shooting technique	An increase in magnetic parameter velocity profile decreases whereas the microrotation profile enhances for N>1 but reverse effect is observed for N<1. Both Dufour and Soret enhance the thermal and concentration boundary layer respectively.
Present work	Study on non-linear boundary value problem for MHD fluid flow with chemical effect	Semi - Analytical	Homotopy analysis approach	High correlation between the semi-analytical and numerical findings of this study. Compared to the prior method, this approach to the model is simpler, and it may be readily extended to find semi-analytical solutions to other MHD and EMHD fluid flow issues in the physical sciences and engineering.

2. Mathematical Formulation of the Problem

As The mixed convection flow of a constant incompressible micropolar fluid between two parallel plates separated by a distance h has been considered. The y-axis is perpendicular to the plates, and the flow direction is along the x-axis. Whereas the fluid's temperature and concentration at the upper plate are and, respectively, those at the lower plate are and (and). A transverse magnetic field is applied with increasing field strength. The heat source and sink, as well as the chemical reaction, are taken into account in the formulas for mass and energy transfer, respectively. The cross-flow velocity of transpiration is constant where denotes the injection velocity and represents the suction velocity.

The equations regulating the flow of incompressible micropolar fluids are [12] under the aforementioned presumptions and Boussinesq approximations with energy and concentrations.

$$v = v_0 = \text{constant} \tag{1}$$

$$\rho v_0 \frac{\partial u}{\partial y} = -\frac{\partial p}{\partial x} + (\mu + k)\frac{\partial^2 u}{\partial y^2} + k.\frac{\partial \Gamma}{\partial y} - \sigma B_0^{\,2} u + \rho g \beta_T (T - T_1) + \rho g \beta_C (C - C_1) \tag{2}$$

$$\rho j v_0 \frac{\partial \Gamma}{\partial y} = \gamma \frac{\partial^2 \Gamma}{\partial y^2} - 2k\rho g\Gamma - k \frac{\partial u}{\partial y} \tag{3}$$

$$c_p \rho v_0 \frac{\partial T}{\partial y} = k_f \frac{\partial^2 T}{\partial y^2} + (\mu + k)\left(\frac{\partial u}{\partial y}\right)^2 + \gamma\left(\frac{\partial \Gamma}{\partial y}\right)^2 + 2\kappa\left(\Gamma^2 + \Gamma\frac{\partial u}{\partial y}\right) + \frac{DK_T}{C_S}\frac{\partial^2 C}{\partial y^2} - q(T - T_\infty) \tag{4}$$

$$v_0 \frac{\partial C}{\partial y} = D\frac{\partial^2 C}{\partial y^2} + \frac{DK_T}{T_m}\frac{\partial^2 C}{\partial y^2} - K c^*(C - C_\infty) \tag{5}$$

where u is velocity components in the x-directions, Γ is micro rotation, ρ and j are the fluid density and gyration parameter, μ, κ, γ are the material constants (viscosity coefficients), g is the acceleration due to gravity, p is pressure, β_T is the coefficient of thermal expansion, β_C is the coefficient of solutal expansion, k_f the coefficient of thermal conductivity, D is the mass diffusivity, c_p is the specific heat of fluid, C_s is the concentration susceptibility, T_m is the mean fluid temperature, and K_T is the thermal diffusion ratio.

The boundary conditions are:

$$u = 0,\ v = v_0, \Gamma = 0, T = T_1, C = C_1,\ \text{at } y = 0 \tag{6}$$

$$u = 0,\ v = v_0, \Gamma = 0, T = T_2, C = C_2,\ \text{at } y = h \tag{7}$$

The following non-dimensional variables are introduced:

$$\eta = \frac{y}{h}, u = U_0\ f(\eta),\ \Gamma = \frac{U_0}{h} w\ (\eta), \quad \theta(\eta) = \frac{T - T_1}{T_2 - T_1},\ \phi(\eta) = \frac{C - C_1}{C_2 - C_1} \tag{8}$$

We obtain the following non-linear system of ordinary differential equations from Eqs. (1) through (5):

$$\frac{1}{N-1} f'' - Rf' + \frac{N}{1-N} w' + \frac{Gr}{\mathrm{Re}}\theta + \frac{Gc}{\mathrm{Re}}\phi - Mf' - A = 0 \tag{9}$$

$$\frac{2-N}{m_p^{\,2}} w'' - a_j \frac{1-N}{N} Rw' - (2w + f') = 0 \tag{10}$$

$$\theta'' - R\,\mathrm{Pr}\,\theta' + \frac{Br}{1-N}\left[f'^2 + \frac{N(2-N)}{m_p^{\,2}} w'^2 + 2N(w^2 - wf')\right] + Du\,\mathrm{Pr}\,\phi'' + \mathrm{Pr}\,\beta\,\theta = 0 \tag{11}$$

$$\frac{1}{Sc}\phi'' - R\phi' + Sr\,\theta'' - \gamma\phi = 0 \tag{12}$$

Where primes denote differentiation with respect to η, $Sc = \frac{v}{D}$ is the Schmidt number, $\mathrm{Pr} = \frac{\mu c_p}{k_f}$ is the Prandtl number, $R_e = \frac{\rho U_0 h}{\mu}$ is the Reynolds number, $Sr = \frac{D K_T (C_2 - C_1)}{v C_s C_p (T_2 - T_1)}$ is the Dufour number, $R = \frac{\rho v_0 h}{\mu}$ is the suction / Injuction parameter, $N = \frac{k}{\mu + k}$ is coupling number, $Gr = \frac{g\rho^2 \beta_T (T_2 - T_1) h^3}{\mu^2}$ is temperature Grashof number, $Gc = \frac{g\rho^2 \beta_c (C_2 - C_1) h^3}{\mu^2}$ is the mass Grashof number, $A = \frac{h^2}{\mu U_0}\frac{dP}{dx}$ is the

constant pressure gradient, $m_p{}^2 = \frac{h^2 k(2\mu + k)}{\gamma(\mu + k)}$ is the micropolar parameter, $a_j = \frac{j}{h^2}$ is the micro-inertial density parameter, $Br = \frac{\mu {U_0}^2}{k_f (T_2 - T_1)}$ is the Brinkman number.

Boundary conditions (6) in terms of f, w, θ, φ become

$$f = 0, w = 0, \ \theta = 0, \ \phi = 0 \qquad at \ \eta = 0 \qquad (13)$$

$$f = 0, w = 0, \ \theta = 1, \ \phi = 1 \qquad at \ \eta = 1 \qquad (14)$$

2.1. Physical Quantities of Interest

The major physical quantities of interest are the skin friction coefficient C_f, Nusselt number Nu, and Sherwood number Sh, which are defined as,

$$C_f = \frac{\tau_w}{\rho {u_m}^2 / 2}, \quad Nu = \frac{x q_w}{k(T_w - T_\infty)}, \quad Sh = \frac{x q_m}{k(C_w - C_\infty)} \qquad (15)$$

Where surface shear stress, Surface heat and mass flux are defined as

$$\tau_w = \left[(\mu + k) \frac{\partial u}{\partial y} + k w \right]_{y=0}, \quad q_w = -k \left(\frac{\partial T}{\partial y} \right)_{y=0}, \quad q_m = -D \left(\frac{\partial C}{\partial y} \right)_{y=0} \qquad (16)$$

Using the non-dimensional variables (8), we get

$$\frac{1}{2} C_f \ {\mathrm{Re}_x}^{1/2} = \left(1 + \frac{K}{2}\right) f'(0), \quad \frac{Nu}{\mathrm{Re}_x{}^{1/2}} = -\theta'(0), \quad \frac{Sh}{\mathrm{Re}_x{}^{1/2}} = -\phi'(0) \qquad (17)$$

3. Semi-Analytical Expressions of the Non-Linear Boundary Value Problem Using the Homotopy Analysis Method

Liao's 1992 invention of the Homotopy analysis method is a noteworthy one for locating answers to non-linear issues. HAM is independent of any small or big physical parameters. Second, HAM offers a practical means of ensuring the convergence of solutions. In conclusion, HAM offers us a practical instrument to resolve extremely non-linear issues in science and engineering.

Consider a differential equation

$$N[f(\eta)] = 0 \qquad (18)$$

where N is a non-linear operator, η denotes independent variable and $f(\eta)$ is a semi-analytical solution of Eq. (17) which is unknown function. Let $f_0(\eta), \ w_0(\eta), \ \theta_0(\eta), \ \phi_0(\eta)$ denote an initial approximations of $f(\eta), \ w(\eta), \ \theta(\eta), \ \phi(\eta)$ respectively. $H(\eta)$ is known as auxiliary function and L denotes an auxiliary linear operator, h is non – zero embedding parameter lies between -1 and 1.

Then the Homotopy is given by,

$$(1-p) \ L[f(\eta); p, h, H(\eta) - f_0(\eta)] = p h \ H(\eta) \ N[f(\eta); p, h, \ H(\eta)] \qquad (19)$$

where $p \in [0, 1]$ is an embedding parameter.

Without having to solve the supplied non-linear problem, we can determine the suitable base functions to represent the answer by evaluating the boundary conditions of the non-linear differential problem.

$$f_0(\eta) = \frac{(1-N)A}{2} \eta + \frac{(N-1)A}{2} \eta^2 \qquad (20)$$

$$w_0(\eta) = 0 \qquad (21)$$

$$\theta_0(\eta) = \eta \qquad (22)$$

$$\phi_0(\eta) = \eta \qquad (23)$$

and the linear operators $L_f, \ L_w, \ L_\theta, \ L_\phi$ are defined as

$$L_f = f'' \qquad (24)$$

$$L_w = w'' \qquad (25)$$

$$L_\theta = \theta'' \qquad (26)$$

$$L_\phi = \phi'' \qquad (27)$$

Applying the Homotopy analysis method,

$$f = \frac{(1-N)A}{2} \eta + \frac{(N-1)A}{2} \eta^2 - h \left[\begin{array}{l} \frac{(N-1)^2 (MA + AR)}{12} \eta \\ + \left(\frac{N}{6} - \frac{1}{6} \right) \left(\frac{Gr}{R} + \frac{Gc}{R} \right) \eta \\ + \left(\begin{array}{l} (N-1)^2 RA - \frac{Gr(N-1)}{R} \\ - \frac{Gc(N-1)}{R} + (N-1)^2 MA \end{array} \right) \frac{\eta^3}{6} \\ - \left(\begin{array}{l} (N-1)^2 RA + \\ (N-1)^2 MA \end{array} \right) \frac{\eta^2}{4} \end{array} \right] \qquad (28)$$

$$w=-h\left[\begin{array}{l}\left[\begin{array}{l}\frac{(1-N)A}{4}\\ -\frac{(1-N)A}{8}\left(\frac{e^{\sqrt{\frac{2}{2-N}}.m_p}+1}{\sinh\sqrt{\frac{2}{2-N}}.m_p}\right)\end{array}\right]\\ e^{\sqrt{\frac{2}{2-N}}.m_p.\eta}\\ +\left[\frac{(1-N)A}{8}\left(\frac{e^{\sqrt{\frac{2}{2-N}}.m_p}+1}{\sinh\sqrt{\frac{2}{2-N}}.m_p}\right)\right]\\ e^{-\sqrt{\frac{2}{2-N}}.m_p.\eta}+\frac{(N-1)A}{4}+\frac{(1-N)A}{2}\eta\end{array}\right] \quad (29)$$

$$\theta=-h\left[\begin{array}{l}\left(\frac{-R\ \mathrm{Pr}}{2}+\frac{3Br(1-N)A^2}{8}\right)\eta\\ +\frac{\mathrm{Pr}\,\beta}{6}\\ +\left(\frac{R\ \mathrm{Pr}}{2}-\frac{Br(1-N)A^2}{8}\right)\eta^2\\ -\left(\frac{Br(1-N)A^2}{12}\right)\eta^4\\ -\left(\frac{Br(1-N)A^2}{6}+\frac{\mathrm{Pr}\,\beta}{6}\right)\eta^3\end{array}\right]+\eta \quad (30)$$

$$\phi=-\left[\begin{array}{l}\frac{RSc\eta}{2}-\frac{\gamma Sc\eta}{6}\\ +\frac{\gamma Sc\eta^3}{6}-\frac{RSc\eta^2}{2}\end{array}\right]h+\eta \quad (31)$$

4. Results and Discussion

In Fig. 1 and Fig. 2 , the fixed parameter values are:

$N=0.5,\ R=2,\mathrm{Pr}=0.71,Gr=0.2,Sc=2,$

$Sr=0.2,\ Gc=2,\ a=1,a_j=0.001,\ \mathrm{Re}=1,\ \gamma=0,$

$m_p=1,Br=1,Du=1,\beta=0,$ where as the varying parameters and its values are given in figures.

Fig. 1 illustrates how a magnetic parameter affects flow phenomena when there is no heat source, no chemical reaction, and other physical parameters present. When data from Dash et al. [12] were compared in the absence of the current discovery, an intriguing observation was found; increasing the magnetic parameter improves the velocity profile by 12.5 % at every site in the velocity boundary layer. For $\eta<0.4$, velocity profile increases as the magnetic parameter increases. After that, it decreases, corresponding to the magnetic parameter. So the variation of the magnetic parameter shows a significant effect on the thickness of the boundary layer.

In Fig. 2 Near the first plate, the micro rotation profile increases by 46.15 % as the magnetic parameter increases; however, the opposite effect is observed after that. The impact of the magnetic parameter on the velocity profiles for N=2.5 is seen in Fig. 3. It can be seen that the effect in this profile is the opposite of what it is in Fig. 1. With an increase in the magnetic parameter, the velocity profile slows down. So the variation of the magnetic parameter does not show a significant effect on the thickness of the boundary layer.

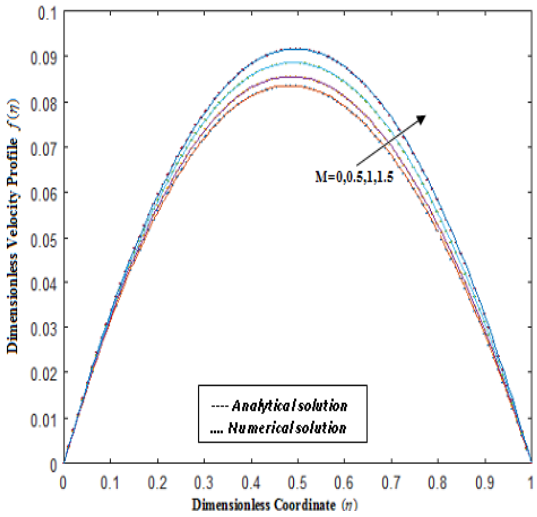

Fig. 1. Dimensionless coordinate η versus the dimensionless velocity profile $f(\eta)$. The curve is plotted using eq. (28). The curve is plotted using eq. (28) for various values of dimensionless parameters and in some fixed values of dimensionless parameters.

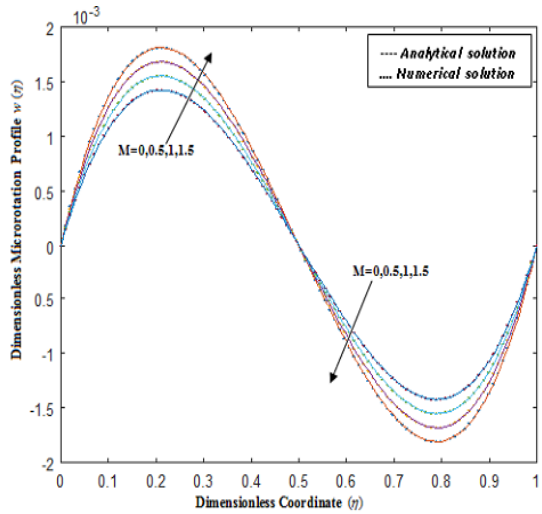

Fig. 2. Dimensionless coordinate η versus the dimensionless micro rotation profile $w(\eta)$. The curve is plotted using eq. (29) for various values of dimensionless parameters and in some fixed values of dimensionless parameters.

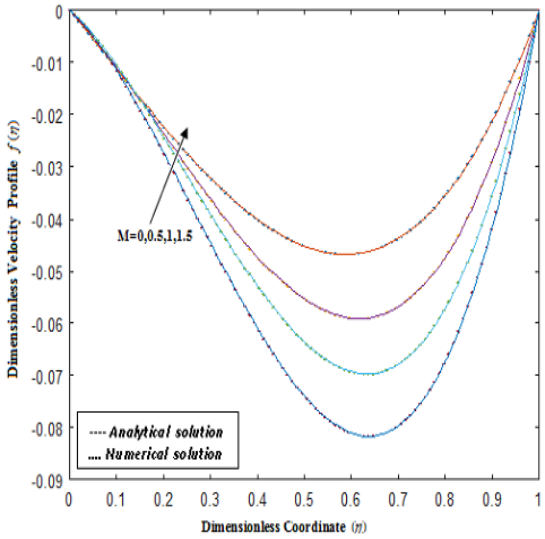

Fig. 3. Dimensionless coordinate η versus the dimensionless velocity profile $f(\eta)$. The curve is plotted using eq. (28) for various values of dimensionless parameter and in some fixed values of dimensionless parameters.

Fig. 4 illustrates how magnetic factors affect the micro rotation profiles for N=2.5. It has been observed that, depending on the micro rotation profile, the intermediate layer of the channel exhibits opposite properties. For the purpose of accommodating the inadequate boundary conditions, the profile slows down before the region and then accelerates after it.

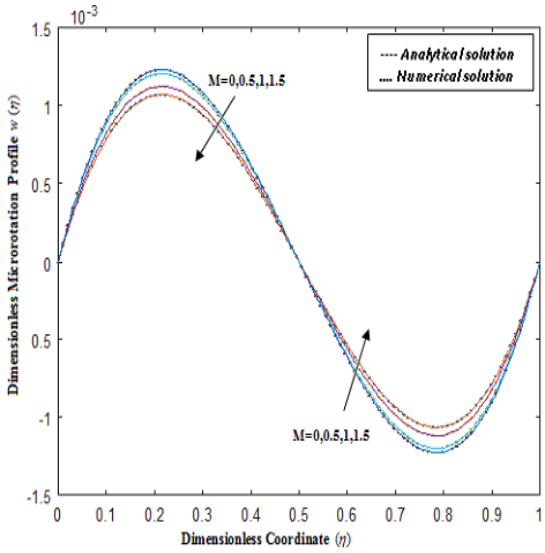

Fig. 4. Dimensionless coordinate η versus the dimensionless micro rotation profile $w(\eta)$. The curve is plotted using eq. (29) for various values of dimensionless parameters and in some fixed values of dimensionless parameters.

Fig. 5 for N = 0.5 illustrates how the thermal and mass buoyancy properties affect the velocity profile that is displayed when magnetic and other parameters are present. It can be seen that the velocity attains its maximum when the thermal buoyancy parameter is 2.0. It is interesting that the increase in thermal and mass buoyancy parameter velocity profile increases significantly. When the buoyancy parameter and the fluid velocity increase, the thermal boundary layer decreases . It causes more fluid in the boundary layer. The Buoyancy effect causes the velocity in the fluid to increase. So there is an increase in higher values of Gr.

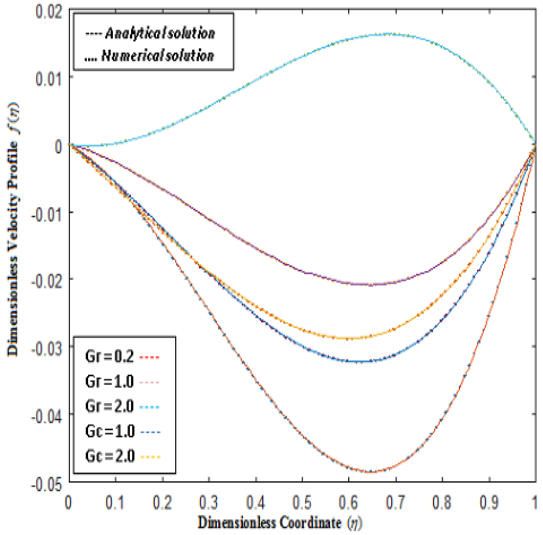

Fig. 5. Dimensionless coordinate η versus the dimensionless velocity profile $f(\eta)$. The curve is plotted using eq. (28) for various values of Gr, Gc and in some fixed values of dimensionless parameters.

The influence of thermal buoyancy and mass buoyancy forces is seen in Fig. 6 (N = 0.5). These forces within the region react negatively, similar to the velocity in Fig. 5, until the trend is reversed.

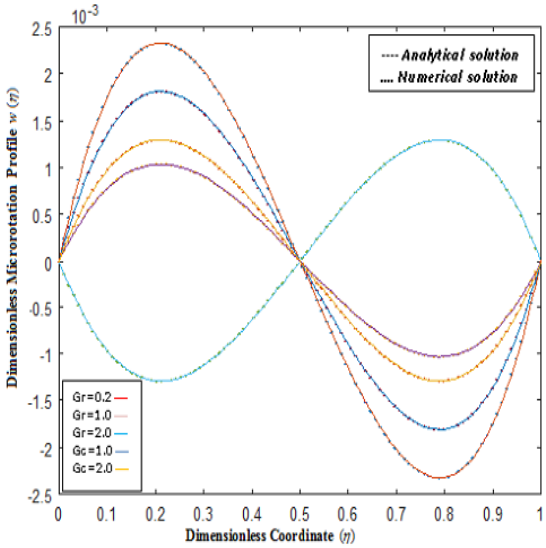

Fig. 6. Dimensionless coordinate η versus the dimensionless micro rotation profile $w(\eta)$. The curve is plotted using eq. (29) for various values of Gr, Gc and in some fixed values of dimensionless parameters.

The temperature profile for N = 2.5 is shown in Fig. 7 as a function of the Prandtl number and the heat generation (source)/absorption (sink) parameter. When it comes to water, the temperature rises when it is near the source and falls when it is near the sink. Stated differently, sink has the opposite effect on the temperature profile. Interestingly, the fluid's temperature increases as the Prandtl number increases. There was not a heat source in one instance. There is good agreement between the present finding and that of [6].

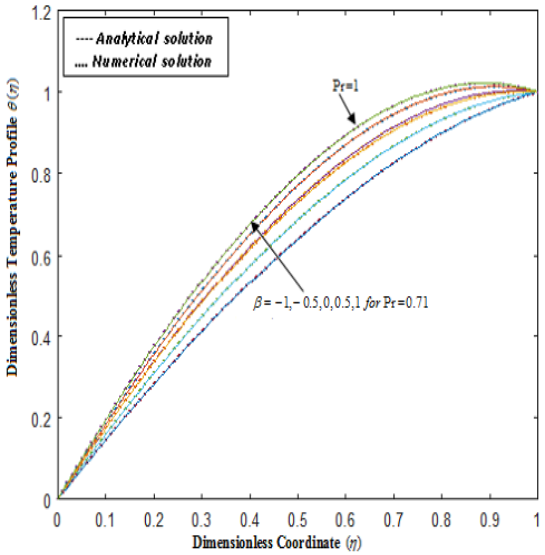

Fig. 7. Dimensionless coordinate η versus the dimensionless temperature profile $\theta(\eta)$. The curve is plotted using eq. (30) for various values of dimensionless parameter and in some fixed values of dimensionless parameters

The coupling number between Figs. 8 and 10 is 0.5. It is significant to observe that in Fig. 8, the fluid temperature rises in tandem with the Dufour number. The presence of a source can raise the fluid temperature of the thermal boundary layer everywhere. Fig. 9 illustrates how the fluid concentration grows with the number of sorets. A high Schmidt number inclusion with a soret number promotes increased fluid concentration by 33.3 % in the concentration boundary layer.

Fig. 10 discusses the consequences of a destructive chemical reaction, a non-chemical reaction, and a constructive chemical reaction. It is clear that the chemical reaction was more significant. As stated otherwise, a destructive chemical reaction causes the fluid concentration to slow down, whereas a constructive reaction results in a negative consequence. In addition, if there is no chemical reaction, the fluid concentration becomes linear. Moreover, the heavier species slow down the fluid concentration at every point in the concentration boundary layer.

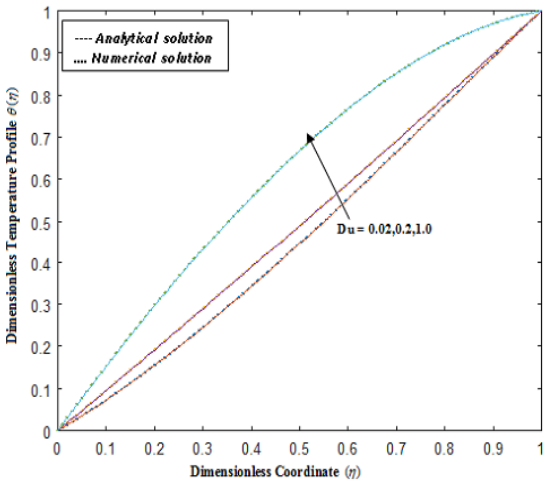

Fig. 8. Dimensionless coordinate η versus the dimensionless temperature profile $\theta(\eta)$. The curve is plotted using eq. (30) for various values of dimensionless parameter and in some fixed values of dimensionless parameters

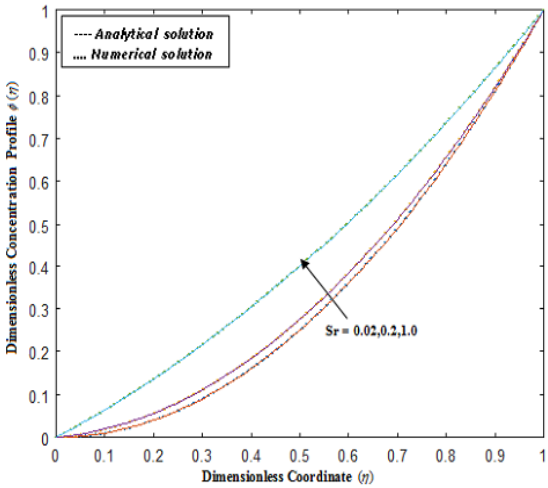

Fig. 9. Dimensionless coordinate η versus the dimensionless concentration profile $\phi(\eta)$. The curve is plotted using eq. (31) for various values of Sr and in some fixed values of dimensionless parameters.

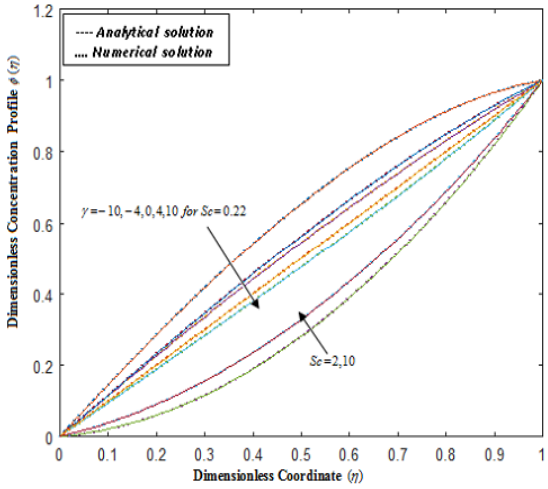

Fig. 10. Dimensionless coordinate η versus the dimensionless concentration profile $\phi(\eta)$. The curve is plotted using eq. (31) for various values of γ, Sc and in some fixed values of dimensionless parameters.

In Fig. 11 and Fig. 14 , the fixed parameter values are:

$N = 2.5, M = 0.5,\ R = 2,\ \Pr = 0.71,\ \mathrm{Re} = 1,$

$Gr = 0.2,\ Gc = 2, Sr = 0.2,$

$\gamma = 0, a = 1, a_j = 0.001, m_p = 1, Br = 1, Du = 1,$

$\beta = 0.\ a_j = 0.001, m_p = 1,\ \gamma = 0, a = 1,$

It should be noted that as the thermal buoyancy parameter rises, the velocity falls, as seen in Fig. 11. The influence of temperature and mass buoyancy forces is shown in Fig. 12. which first react in the opposite way inside the region as that of velocity in Fig. 6 before trending in the opposite direction. Fig. 13 illustrates how the fluid concentration increases in proportion to the Soret number. A high Schmidt number inclusion with Soret number promotes increased fluid concentration in the concentration boundary layer.

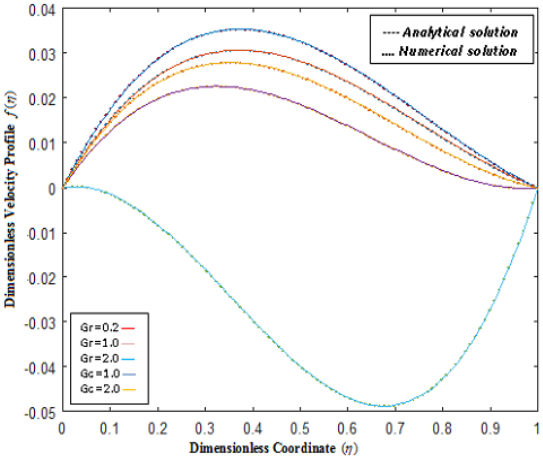

Fig. 11. Dimensionless coordinate η versus the dimensionless velocity profile $f(\eta)$. The curve is plotted using Eq. (28) for various values of Gr, Gc and in some fixed values of dimensionless parameters.

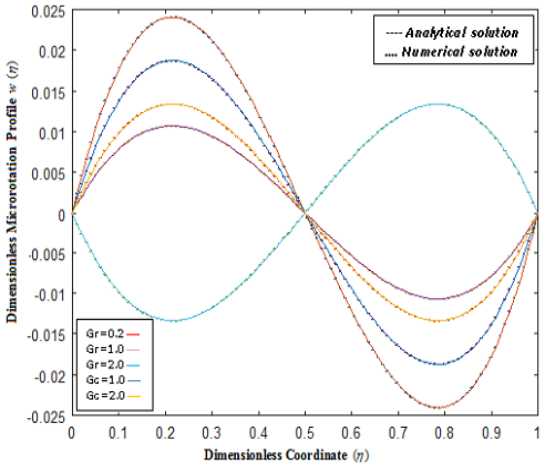

Fig. 12. Dimensionless coordinate η versus the dimensionless micro rotation profile $w(\eta)$. The curve is plotted using Eq. (29) for various values of Gr, Gc and in some fixed values of dimensionless parameters.

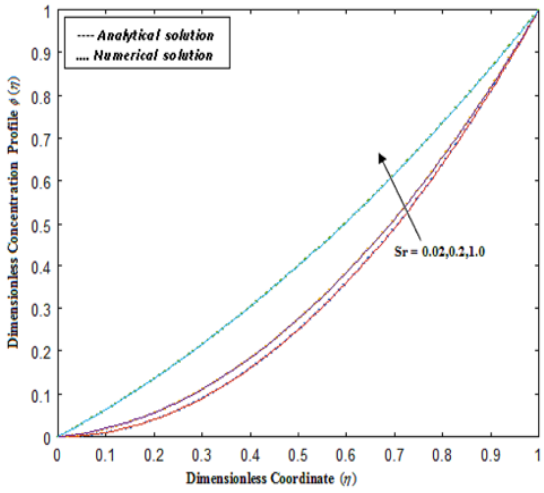

Fig. 13. Dimensionless coordinate η versus the dimensionless concentration profile $\phi(\eta)$. The curve is plotted using eq. (31) for various values of Sr and in some fixed values of dimensionless parameters.

Fig. 14 illustrates the consequences of a destructive chemical reaction, a non-chemical reaction, and a constructive chemical reaction. It is clear that the chemical reaction was more significant. As stated otherwise, a destructive chemical reaction causes the fluid concentration to slow down, whereas a constructive reaction results in a negative consequence. In addition, if there is no chemical reaction, the fluid concentration becomes linear. Moreover, the heavier species slow down the fluid concentration at every point in the concentration boundary layer.

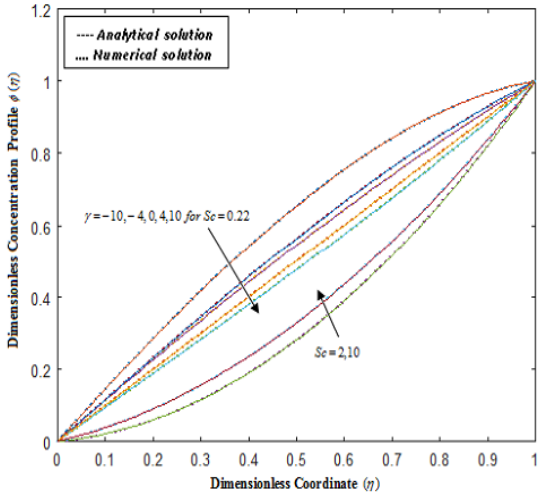

Fig. 14. Dimensionless coordinate η versus the dimensionless concentration profile $\phi(\eta)$. The curve is plotted using eq. (31) for various values of γ, Sc and in some fixed values of dimensionless parameters.

The temperature profile for N = 0.5, is influenced by the Prandtl number and the heat generation (source) / absorption (sink)

parameters, as illustrated in Fig. 15. When it comes to water, temperature increases occur in the source while temperature drops in the sink. As stated differently, the sink has the opposite effect on the temperature profile. Interestingly, the fluid's temperature increases as the Prandtl number increases. There was not a heat source in one instance. There is good agreement between the present finding and that of [6]. It's noteworthy to see that in Fig. 16, the fluid temperature raises in tandem with the Dufour number by 66%. The fluid temperature of the thermal boundary layer can always be raised by the presence of a source at N = 2.5.

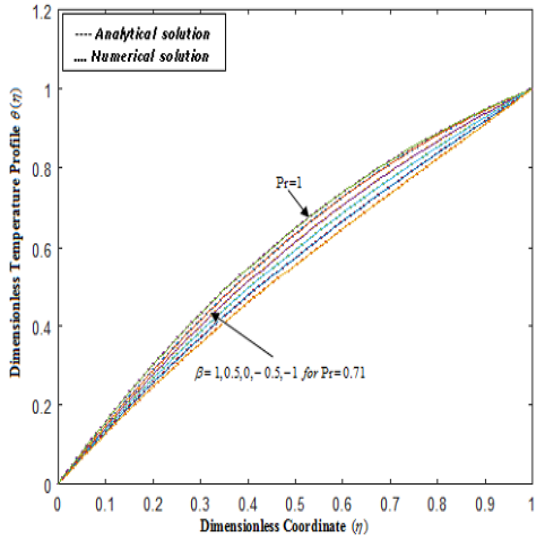

Fig. 15. Dimensionless coordinate η versus the dimensionless temperature profile $\theta(\eta)$. The curve is plotted using eq. (30) for various values of dimensionless parameter and in some fixed values of dimensionless parameters.

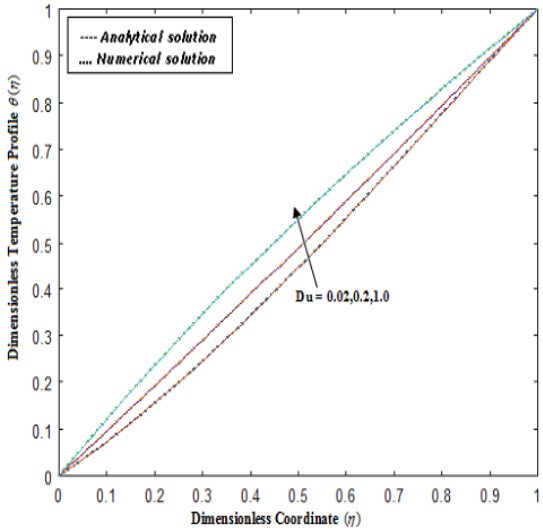

Fig. 16. Dimensionless coordinate η versus the dimensionless temperature profile $\theta(\eta)$. The curve is plotted using eq. (30) for various values of dimensionless parameter and in some fixed values of dimensionless parameters.

The impact of Re and N on Skin friction coefficient is presented in Fig. 17. Skin friction coefficient In both cases ($M > 0$ and $M < 0$), the Skin friction coefficient decays with an increment in the coupling number (N) and Reynolds number (Re). Fig. 18 represents the effect of Gr and K. Increasing the value of temperature, Grashof number and coefficient of thermal conductivity, elevates the Skin friction coefficient. The values are given in Table 2. It is observed that the increasing value of the magnetic parameter, thermal and solutal buoyancy, decreases the skin friction in magnitude whereas an increase in the material parameter, N increases the skin friction coefficient.

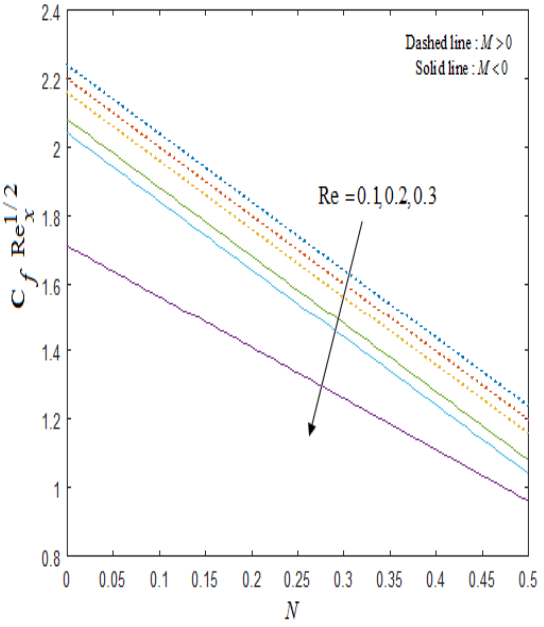

Fig. 17. Impact of Re and N versus Skin friction.

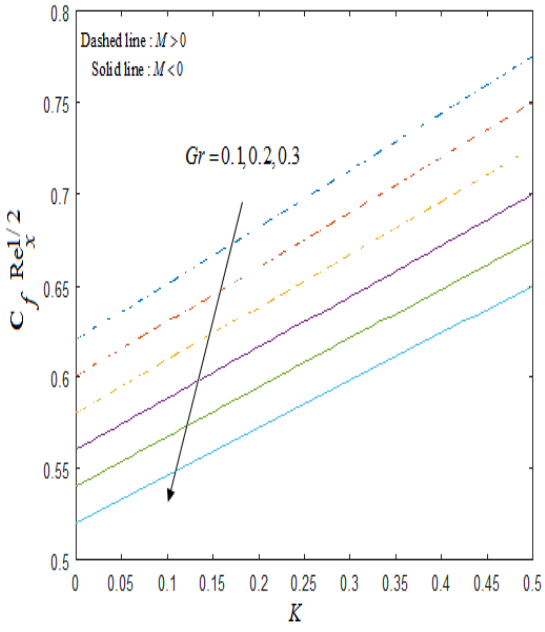

Fig. 18. Impact of Gr and K versus Skin friction.

Table 2. The Skin Friction Coefficient $f'(0)$ are given as follows:

N, Gr, Gc, A, R	M	0.5	1.5	2.5
	Numerical Solution	- 0.157892	- 0.155528	-0.154781
	Analytical Solution	- 0.157889	- 0.155412	-0.153217
	Error	0.000003	0.0000116	0.001564
M, Gr, Gc, A, R	N	0.5	1.5	2.5
	Numerical Solution	- 0.154896	-0.414134	- 0.669917
	Analytical Solution	- 0.154790	-0.401781	- 0.669906
	Error	0.000106	0.012353	0.000011
M, N, Gc, A, R	Gr	0.2	1	2
	Numerical Solution	- 0.154896	-0.065104	- 0.038694
	Analytical Solution	- 0.153712	-0.062561	- 0.037584
	Error	0.001184	0.002543	0.001110
M, N, Gr, A, R	Gc	1	2	3
	Numerical Solution	-0.171851	- 0.154896	- 0.137380
	Analytical Solution	-0170750	- 0.153128	- 0.136120
	Error	0.001101	0.001768	0.001260
M, N, Gr, Gc, A	R	2	3	4
	Numerical Solution	- 0.154884	- 0.136780	-0.111598
	Analytical Solution	- 0.154881	- 0.136618	-0.110130
	Error	0.000003	0.000162	0.001468
M, N, Gr, Gc, R	A	1	2	3
	Numerical Solution	- 0.172392	- 0.142189	-0.126590
	Analytical Solution	- 0.172100	- 0.141080	-0.124318
	Error	0.000292	0.001109	0.002272

The variations of Nu for different combinations of R and N is illustrated in Fig. 19. For small variations in the coupling number (N) and suction/Injuction parameter (R), there is a fall in the Nusselt number. The influence of Br and Pr on the Nusselt number is studied in Fig. 20. On varying the Brinkman number from 0 to 2 with respect to the Prandtl numbers 0.71, 0.81, 0.91, then the Nusselt number gets increasing by 33.33%. The values are given in Table 3. The Nusselt number is significantly affected by suction/injection parameter.

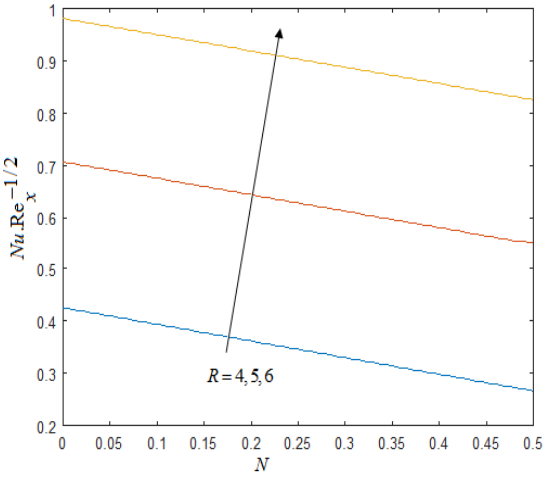

Fig. 19. Impact of R and N versus Nusselt Number.

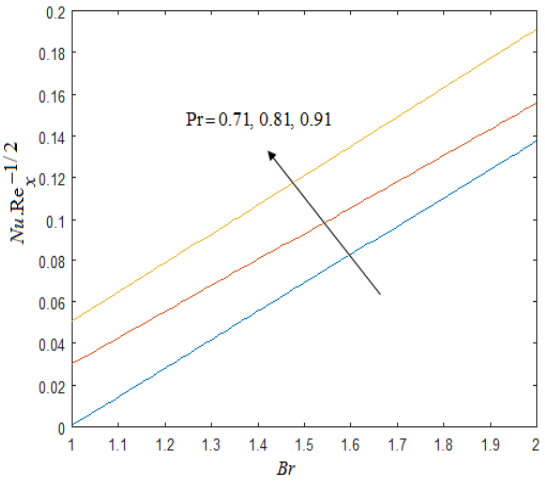

Fig. 20. Impact of Br and Pr versus Nusselt Number.

The effect of R and Sc on the Sherwood number is shown in Fig. 21. The Schmidt number shows a rapid increase on varying R from 2 to 8, whereas it shows a little variation when increasing Sc from 2 to 4. Fig. 22 explains the variation of R and γ when the Sherwood number. From the Fig., it can be concluded that for fixed $R=8$ and varying $\gamma=0,4,10$, the Sherwood number remains 0. After that stage (i.e. for R = 8 to 9), the Sherwood number rises. The values are given in Table 4.

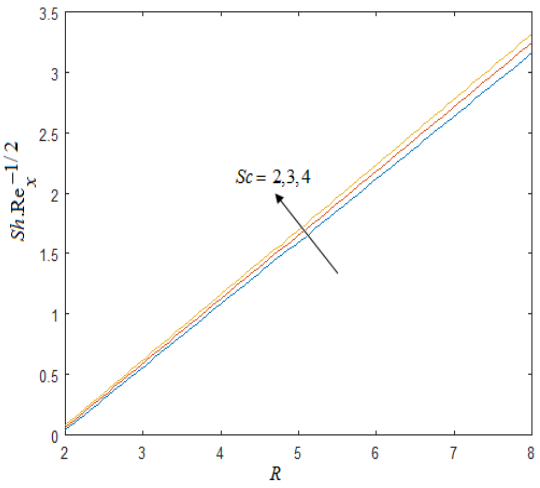

Fig. 21. Impact of R and Sc versus Sherwood Number.

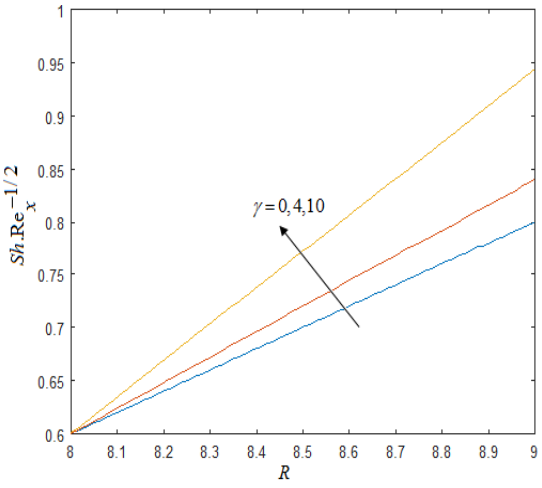

Fig. 22. Impact of R and γ versus Sherwood Number.

Table 3. The Nusselt Number $-\theta'(0)$ are given as follows:

	N	0.5	1.5	2.5
	Numerical Solution	0.820560	0.805481	0.788503
R, Pr, Br, A, β	Analytical Solution	0.820410	0.803210	0.788502
	Error	0.000150	0.002271	0.000001
	β	0	-1	1
	Numerical Solution	0.818349	0.749083	0.821786
N, R, Pr, Br, A	Analytical Solution	0.817218	0.748072	0.810634
	Error	0.001131	0.001011	0.011152
	Pr	0.71	0.81	0.91
	Numerical Solution	0.821877	0.758125	0.731681
N, R, Br, A, β	Analytical Solution	0.810811	0.748615	0.720623
	Error	0.010066	0.009510	0.011058

Table 4. The Sherwood Number $-\varphi'(0)$ are given as follows:

	Sc	2	3	4
	Numerical Solution	0.166015	0.167984	0.168123
R, γ	Analytical Solution	0.165923	0.156321	0.167121
	Error	0.000092	0.011663	0.001002
	γ	0	-1	1
	Numerical Solution	0.157014	0.176388	0.156002
R, Sc	Analytical Solution	0.146901	0.175123	0.155013
	Error	0.010113	0.001265	0.000989

5. Conclusions

The non-linear boundary value problem for MHD micropolar fluid between two parallel plates in the presence of a heat source and sink has been studied using a semi-analytical technique in this study. HAM solved the governing equations. The conclusions that follow are drawn.

1. For N>1, the micro rotation profile increases while the magnetic parameter velocity profile falls; for N<1, the opposite impact is seen.
2. Maximum velocity occurs at higher buoyant force values.
3. The thermal and concentration boundary layers are both strengthened by Dufour and Soret, respectively.
4. The concentration profile is retarded by heavier species as well as chemical reactions.
5. While the rate of mass transfer increases, the skin friction coefficient and heat transfer rate decrease with an increase in N.

6. While the skin friction coefficient rises with an increase in material parameter N, the skin friction magnitude reduces with an increase in magnetic parameter, temperature, and solutal buoyancy values.
7. The rate of heat transmission is decreased by all parameters other than the heat source and the destructive chemical reaction, but the rate of mass transfer exhibits the opposite effect.

We notice that the numerical approach is convenient and closed when we compare our stated outcomes to it. The purpose of obtaining the graphical findings was to examine the effects of multiple parameters. The study's findings were generally consistent with those of earlier investigations.

Comparing our stated results to the numerical approach, we find that it is closed and convenient. The graphical results were obtained in order to study the consequences of several parameters. The research results were in good agreement with the results of previous work.

Nomenclature

Symbol	Meaning
C	Fluid concentration
D	Coefficient of the mass diffusivity
A	Constant Pressure gradient
Pr	Prandtl number
Br	Brinkman number
g	Acceleration due to gravity
M	Magnetic parameter
N	Coupling number
k	Material parameter
C_p	Specific molecular diffusivity
Sc	Schmidt number
C_f	Skin friction coefficient
$\theta(\eta)$	Dimensionless temperature
T	Fluid temperature
μ	Dynamic viscosity
T_∞	Fluid temperature at infinity
δ	Solutal buoyancy parameter
B_0	Magnetic flux density
α	Thermal diffusivity
Sh	Sherwood number
σ	Electrical conductivity
k_f	Thermal conductivity
λ	Thermal buoyancy or mixed convection parameter
Nu	Nusselt number
Gr	Temperature Grashof number
Gc	Mass Grashof number
ρ	Density of the fluid
u, v	Velocity components along x- and y-direction
κ	Vortex viscosity or micro rotation viscosity
j	Micro-inertia density
C_w	Stretching sheet concentration
Ec	Eckert number
T_w	Stretching sheet temperature
x, y	Coordinates
γ	Chemical reaction parameter
ν	Kinematic viscosity
C_1	Species concentration at upper plate
β	heat source / sink parameter
ω	Angular velocity or micro rotation vector
$\phi(\eta)$	Non-dimensional concentration parameter
$f(\eta)$	Non-dimensional velocity parameter

Acknowledgments

The authors are thankful to Sri. S. Natanagopal, Secretary, The Madura College board, Dr. J. Suresh, The Principal, The Madura College and Dr. C. Thangapandi, Head of the Department, The Madura College, Madurai, Tamil Nadu, India for their constant support to our research work.

Funding Statement

This research did not receive any specific grant from funding agencies in the public, commercial, or not-for-profit sectors.

Conflicts of Interest

The author declares that there is no conflict of interest regarding the publication of this article.

Appendix

Appendix-A: Semi-Analytical Solution of the Non-Linear Boundary Value Problem Using the Homotopy Analysis Method

The given non-linear differential equations are

$$f'' - R(N-1)f' + Nw' + \frac{Gr}{\mathrm{Re}}(N-1)\theta + \frac{Gc}{\mathrm{Re}}(N-1)\phi - M(N-1)f' - A(N-1) = 0 \quad \text{(A.1)}$$

$$w'' - a_j \frac{1-N}{N}.\frac{m_p{}^2}{2-N}Rw' - 2w.\frac{m_p{}^2}{2-N} - \frac{m_p{}^2}{2-N}f' = 0 \quad \text{(A.2)}$$

$$\theta'' - R\,\mathrm{Pr}\,\theta' + \frac{Br}{1-N}\begin{bmatrix} f'^2 + \dfrac{N(2-N)}{m_p{}^2}w'^2 \\ +2N(w^2 - wf') \end{bmatrix} + Du\,\mathrm{Pr}\,\phi'' + \mathrm{Pr}\,\beta\,\theta = 0 \quad \text{(A.3)}$$

$$\phi'' - Sc\,R\phi' + Sc\,Sr\,\theta'' - Sc\,\gamma\,\phi = 0 \quad \text{(A.4)}$$

with the boundary conditions

$$f = 0, w = 0,\ \theta = 0,\ \phi = 0 \qquad at\ \eta = 0 \quad \text{(A.5)}$$

$$f = 0, w = 0,\ \theta = 1,\ \phi = 1 \qquad at\ \eta = 1 \quad \text{(A.6)}$$

We construct the Homotopy for the Eqs. (A. 1) to (A. 4) are as follows :

$$(1-p)\left[f'' - (N-1)A\right] + \begin{bmatrix} f'' - R(N-1)f' + Nw' \\ +\dfrac{Gr}{\mathrm{Re}}(N-1)\theta + \dfrac{Gc}{\mathrm{Re}}(N-1)\phi \\ -M(N-1)f' - A(N-1) \end{bmatrix} = 0 \quad \text{(A.7)}$$

$$(1-q)w'' + q\begin{bmatrix} w'' - a_j\dfrac{1-N}{N}.\dfrac{m_p{}^2}{2-N}Rw' \\ -2w.\dfrac{m_p{}^2}{2-N} - \dfrac{m_p{}^2}{2-N}f' \end{bmatrix} = 0 \quad \text{(A.8)}$$

$$(1-r)\theta'' + r\begin{bmatrix} \theta'' - R\,\mathrm{Pr}\,\theta' \\ +\dfrac{Br}{1-N}\begin{bmatrix} f'^2 + \dfrac{N(2-N)}{m_p{}^2}w'^2 \\ +2N(w^2 - wf') \end{bmatrix} \\ +Du\,\mathrm{Pr}\,\phi'' + \mathrm{Pr}\,\beta\,\theta \end{bmatrix} = 0 \quad \text{(A.9)}$$

$$(1-s)\phi'' + s\left[\phi'' - Sc\,R\phi' + Sc\,Sr\,\theta'' - Sc\,\gamma\,\phi\right] = 0 \quad \text{(A.10)}$$

The semi-analytical expressions of the equations of (A.1) to (A.4) are as follows:

$$f = f_0 + p\,f_1 + p^2 f_2 + p^3 f_3 + \ldots \quad \text{(A.11)}$$

$$w = w_0 + q\,w_1 + q^2 w_2 + q^3 w_3 + \ldots \quad \text{(A.12)}$$

$$\theta = \theta_0 + r\,\theta_1 + r^2\theta_2 + r^3\theta_3 + \ldots \quad \text{(A.13)}$$

$$\phi = \phi_0 + s\,\phi_1 + s^2\phi_2 + s^3\phi_3 + \ldots \quad \text{(A.14)}$$

Substituting the Eqs. (A.11) to (A.14) in the Eqs. (A.7) to (A.10) respectively and comparing the coefficients of the powers of p, q, r, s we get,

$$p^0 \ :\ f_0'' - (N-1)A = 0 \quad \text{(A.15)}$$

$$p^1 \ :\ f_1'' - R(N-1)f_0' + Nw_0' + \frac{Gr}{\mathrm{Re}}(N-1)\theta_0 + \frac{Gc}{\mathrm{Re}}(N-1)\phi_0 - M(N-1)f_0' = 0 \quad \text{(A.16)}$$

$$q^0 \ :\ w_0'' = 0 \quad \text{(A.17)}$$

$$q^1 \ :\ w_1'' - a_j\frac{1-N}{N}.\frac{m_p{}^2}{2-N}Rw_0' - 2w_0.\frac{m_p{}^2}{2-N} - \frac{m_p{}^2}{2-N}f_0' \quad \text{(A.18)}$$

$$r^0 \ :\ \theta_0'' = 0 \quad \text{(A.19)}$$

$$r^1 \ :\ \theta_1'' - R\,\mathrm{Pr}\,\theta_0' + \frac{Br}{1-N}\begin{bmatrix} f_0'^2 + \dfrac{N(2-N)}{m_p{}^2}w_0'^2 \\ +2N(w_0'^2 - w_0 f_0') \end{bmatrix} + Du\,\mathrm{Pr}\,\phi_0'' + \mathrm{Pr}\,\beta\,\theta_0 = 0 \quad \text{(A.20)}$$

$$s^0 \ :\ \phi_0'' = 0 \quad \text{(A.21)}$$

$$s^1 \ :\ \phi_1'' - Sc\,R\phi_0' + Sc\,Sr\,\theta_0'' - Sc\,\gamma\,\phi_0 = 0 \quad \text{(A.22)}$$

The initial approximations are as follows :

$$f_0(0) = 0,\ f_i(0) = 0, \qquad i = 1, 2, 3, \ldots. \quad \text{(A.23)}$$

$$w_0(0) = 0,\ w_i(0) = 0, \qquad i = 1, 2, 3, \ldots. \quad \text{(A.24)}$$

$$\theta_0(0) = 0,\ \theta_i(0) = 0, \qquad i = 1, 2, 3, \ldots. \quad \text{(A.25)}$$

$$\phi_0(0) = 0,\ \phi_i(0) = 0, \qquad i = 1, 2, 3, \ldots. \quad \text{(A.26)}$$

$$f_0(1) = 0, \quad f_i(1) = 0, \quad i = 1, 2, 3, \ldots. \quad \text{(A.27)}$$

$$w_0(1) = 0, \quad w_i(1) = 0, \quad i = 1, 2, 3, \ldots. \quad \text{(A.28)}$$

$$\theta_0(1)=1,\quad \theta_i(1)=0,\quad i=1,2,3,\ ....\tag{A.29}$$

$$\phi_0(1)=1,\quad \phi_i(1)=0,\quad i=1,2,3,\ ....\tag{A.30}$$

$$f_0(\eta)=\frac{(1-N)A}{2}.\eta+\frac{(N-1)A}{2}.\eta^2\tag{A.31}$$

$$\begin{aligned}f_1(\eta)=&\frac{(N-1)^2(MA+AR)}{12}\eta\\&+\left(\frac{N}{6}-\frac{1}{6}\right)\left(\frac{Gr}{R}+\frac{Gc}{R}\right)\eta\\&+\begin{pmatrix}(N-1)^2RA-\dfrac{Gr(N-1)}{R}\\-\dfrac{Gc(N-1)}{R}+(N-1)^2MA\end{pmatrix}\frac{\eta^3}{6}\\&-\left((N-1)^2RA+(N-1)^2MA\right)\frac{\eta^2}{4}\end{aligned}\tag{A.32}$$

$$w_0(\eta)=0\tag{A.33}$$

$$\begin{aligned}w_1(\eta)=&C_1\ e^{\sqrt{\frac{2}{2-N}}.m_p.\eta}+C_2e^{-\sqrt{\frac{2}{2-N}}.m_p.\eta}\\&+\frac{(N-1)A}{4}+\frac{(1-N).A.\eta}{2}\end{aligned}\tag{A.34}$$

where

$$\begin{aligned}C_1=&\frac{(1-N)A}{4}\\&-\frac{(1-N)A}{8}\left(\frac{e^{\sqrt{\frac{2}{2-N}}.m_p}+1}{\sinh\sqrt{\frac{2}{2-N}}.m_p}\right),\end{aligned}\tag{A.35}$$

$$C_2=\frac{(1-N)A}{8}\left(\frac{e^{\sqrt{\frac{2}{2-N}}.m_p}+1}{\sinh\sqrt{\frac{2}{2-N}}.m_p}\right)$$

$$\theta_0(\eta)=\ \eta\tag{A.36}$$

$$\begin{aligned}\theta_1(\eta)=&\left(\begin{matrix}\dfrac{-R\ \Pr}{2}+\dfrac{\Pr\beta}{6}\\+\dfrac{3Br(1-N)A^2}{8}\end{matrix}\right)\eta\\&+\left(\frac{R\ \Pr}{2}-\frac{Br(1-N)A^2}{8}\right)\eta^2\\&-\left(\frac{Br(1-N)A^2}{12}\right)\eta^4\\&-\left(\frac{Br(1-N)A^2}{6}+\frac{\Pr\beta}{6}\right)\eta^3\end{aligned}\tag{A.37}$$

$$\phi_0(\eta)=\eta\tag{A.38}$$

$$\phi_1(\eta)=\frac{R\,Sc\,\eta}{2}-\frac{\gamma\,Sc\,\eta}{6}+\frac{\gamma\,Sc\,\eta^3}{6}-\frac{R\,Sc\,\eta^2}{2}\tag{A.39}$$

According to HAM, for $-1\le h\le 1$, as $p\to 1$, $q\to 1$, $r\to 1$, $s\to 1$we acquire the following:

$$f=\lim_{p\to 1}\ f(\eta)=\ f_0-h\ f_1\tag{A.40}$$

$$w=\lim_{q\to 1}\ w(\eta)=\ w_0-h\,w_1\tag{A.41}$$

$$\theta=\lim_{r\to 1}\ \theta(\eta)=\ \theta_0-h\,\theta_1\tag{A.42}$$

$$\phi=\lim_{s\to 1}\ \phi(\eta)=\ \phi_0-h\,\phi_1\tag{A.43}$$

Substituting Eqs. (A.31) to (A.39) into Eqs. (A.40) to (A.43), we obtain the results in the text Eqs. (28) to (31) respectively.

References

[1] Eringen, A.C., 1966. Theory of micropolar fluids. *Journal of mathematics and Mechanics*, pp.1-18.

[2] Mishra, S.R., Dash, G.C. and Pattnaik, P.K., 2015. Flow of heat and mass transfer on MHD free convection in a micropolar fluid with heat source. *Alexandria Engineering Journal*, *54*(3), pp.681-689.

[3] Haque, M.Z., Alam, M.M., Ferdows, M. and Postelnicu, A., 2012. Micropolar fluid behaviors on steady MHD free convection and mass transfer flow with constant heat and mass fluxes, joule heating and viscous dissipation. *Journal of King Saud University-Engineering Sciences*, *24*(2), pp.71-84.

[4] Rahman, M.M., Aziz, A. and Al-Lawatia, M.A., 2010. Heat transfer in micropolar fluid along an inclined permeable plate with variable fluid properties. *International Journal of thermal sciences*, *49*(6), pp.993-1002.

[5] Aurangzaib, Kasim, A.R.M., Mohammad, N.F. and Shafie, S., 2013. Unsteady MHD mixed convection flow of a micropolar fluid along an inclined stretching plate. *Heat Transfer—Asian Research*, *42*(2), pp.89-99.

[6] Srinivasacharya, D. and Bindu, K.H., 2016. Entropy generation in a micropolar fluid flow through an inclined channel. *Alexandria engineering journal*, *55*(2), pp.973-982.

[7] Ananthaswamy, V., Nithya, T. and Santhi, V.K., 2019. A Mathematical study on MHD pIane Poiseuille flow in a porous channel with non-uniform plate temperature. *Journal of Applied Science and Computations*, *6*(3), pp.1178-1194.

[8] Sekhar, B.C., Kumar, P.V. and Veera Krishna, M., 2023. Changeable Heat and Mass Transport on Unsteady MHD Convective Flow Past an Infinite Vertical Porous Plate. *Journal of Heat and Mass Transfer Research*, *10*(2), pp.207-222.

[9] El Hamma, M., Aberdane, I., Taibi, M., Rtibi, A. and Gueraoui, K., 2023. Analysis of MHD thermosolutal convection in a porous cylindrical cavity filled with a Casson nanofluid, considering Soret and Dufour effects. *Journal of Heat and Mass Transfer Research*, *10*(2), pp.197-206.

[10] Meenakshi, V., 2021. Dufour and Soret Effect on Unsteady MHD Free Convection and Mass Transfer Flow Past an Impulsively Started Vertical Porous Plate Considering with Heat Generation. *Journal of Heat and Mass Transfer Research*, *8*(2), pp.257-266..

[11] Swapna, D., Govardhan, K., Narender, G. and Misra, S., 2023. Viscous Dissipation and Chemical Reaction on Radiate MHD Casson Nanofluid Past a Stretching Surface with a Slip Effect. *Journal of Heat and Mass Transfer Research*, *10*(2), pp.315-328.

[12] Dash, A.K., Mishra, S.R. and Acharya, B.P., 2017. Chemical reaction effect of MHD micropolar fluid flow between two parallel plates in the presence of heat source/sink. *Model Measurement Control B*, *86*(3), pp.593-608.

[13] Rafiq, M., Rehman, A., Sheikh, N., Saleem, M., Umar Farooq, M., 2023. Numerical Study of the Boundary Layer Flow Problem over a Flat Plate by Finite Difference Method. *Applied Engineering*, *7*(2), pp. 27-36.

[14] Oyelami, F.H., Olumide, F.B., Olubunmi, I.E. and Yetunde, S.B.O., 2024. Numerical Study of Chemical Reaction and Magnetic Field Effects on MHD Boundary Layer Flow over a Flat Plate. *CFD Letters*, *16*(3), pp.55-68.

[15] Mehala, N. and Rajendran, L., 2014. Analysis of mathematical modelling on potentiometric biosensors. *International Scholarly Research Notices*, *2014*(1), p.582675.

[16] Shirly, P.F., Narmatha, S. and Rajendran, L., 2013. Analytical solution of boundary value problem in reactive gas absorption. *International Journal of Mathematical Archive-4 (6)*, pp.228-242.

[17] Ananthaswamy, V. and Rajendran, L., 2012. Analytical solutions of some two-point non-linear elliptic boundary value problems.

[18] Rasi, M., Rajendran, L. and Subbiah, A., 2015. Analytical expression of transient current-potential for redox enzymatic homogenous system. *Sensors and Actuators B: Chemical*, *208*, pp.128-136.

[19] Liao, S.J., 1995. An approximate solution technique not depending on small parameters: a special example. *International Journal of Non-Linear Mechanics*, *30*(3), pp.371-380.

[20] Ananthaswamy, V. and Rajendran, L., 2012. Approximate analytical solution of non-linear kinetic equation in a porous pellet. *Global Journal of pure and applied mathematics*, *8*(2), pp.101-111.

[21] Subanya, R.R., Ananthaswamy, V. and Sivasundaram, S., 2023. Semi analytical expressions of a non-linear boundary value problem for immobilized enzyme in porous planar, cylindrical and spherical. *Nonlinear Studies*, *30*(1).

[22] Wazwaz, A.M., 2014. The variational iteration method for solving linear and nonlinear ODEs and scientific models with variable coefficients. *Central European Journal of Engineering*, *4*, pp.64-71.

[23] He, J.H., 1999. Homotopy perturbation technique. *Computer methods in applied mechanics and engineering*, *178*(3-4), pp.257-262.

[24] He, J.H., 2003. Homotopy perturbation method: a new nonlinear analytical technique. *Applied Mathematics and computation*, *135*(1), pp.73-79.

[25] Mousaa, M.M. and Ragab, S.F., 2008. Application of the homotopy perturbation method to linear and nonlinear schrödinger equations. *Zeitschrift für Naturforschung A*, *63*(3-4), pp.140-144.

[26] Shanthi, D., Ananthaswamy, V. and Rajendran, L., 2013. Analysis of non-linear reaction-diffusion processes with Michaelis-Menten kinetics by a new Homotopy perturbation method.

[27] Shirly Peace, F., Sathiyaseelan, N. and Rajendran, L., 2014. Analytical Solution of Nonlinear Dynamics of a Self-Igniting Reaction-Diffusion System Using Modified Adomian Decomposition Method. *International Journal of Chemical Engineering*, *2014*(1), p.825797.

[28] Liao, S., 2004. On the homotopy analysis method for nonlinear problems. *Applied mathematics and computation*, *147*(2), pp.499-513.

[29] Ananthaswamy, D.V. and Kala, S., 2014. L. Rajendran Approximate analytical solution of non-linear initial value problem for an autocatalysis in a continuous stirred tank reactor: Homotopy analysis method. *International Journal of Mathematical Archive*, *5*(4), pp.1-12.

[30] Anantliaswamy, V., Nithya, T. and Santhi, V.K., 2019. Approximate analytical expressions of a boundary layer flow of viscous fluid using the modified Homotopy analysis method. *Journal of Information and Computational Sciences*, *9*(8), pp.534-541.

[31] Nisar, K.S., Mohapatra, R., Mishra, S.R. and Reddy, M.G., 2021. Semi-analytical solution of MHD free convective Jeffrey fluid flow in the presence of heat source and chemical reaction. *Ain Shams Engineering Journal*, *12*(1), pp.837-845.

[32] Sivasankari, S., Ananthaswamy, V. and Sivasundaram, S., 2023. A new approximate analytical method for solving some non-linear initial value problems in physical sciences. *Mathematics in Engineering, Science & Aerospace (MESA)*, *14*(1).

[33] Chitra, J., Ananthaswamy, V., Sivasankari, S. and Sivasundaram, S., 2023. A new approximate analytical method (ASM) for solving non-linear boundary value problem in heat transfer through porous fin. *Mathematics in Engineering, Science & Aerospace (MESA)*, *14*(1).

[34] Venugopal, K., Eswari, A. and Rajendran, L., 2011. Mathematical model for steady state current at PPO-modified micro-cylinder biosensors. *Journal of Biomedical Science and Engineering*, *4*(09), p.631.

[35] Ananthaswamy, V. and Narmatha, S., 2019. Comparison between the new Homotopy perturbation method and modified Adomain decomposition method in solving a system of non-linear self igniting reaction diffusion equations. *International Journal of Emerging Technologies and Innovative Research (www. jetir. org), ISSN*, pp.2349-5162.

[36] Sharma, S. and Jain, S., 2024. Chemical Reactions on MHD Couple Stress Fluids towards Stretchable Inclined Cylinder. *Journal of Heat and Mass Transfer Research*.

[37] Konwar, H., 2022. Flow, Heat and Mass Transfer past a Stretching Sheet with Temperature Dependent Fluid Properties in Porous Medium. *Journal of Heat and Mass Transfer Research*, *9*(1), pp.17-26.